ACS OMEGA

Open Access

http://pubs.acs.org/journal/acsodf

Article

Adaptations of *Escherichia coli* K 12 to Synchrotron Sourced THz Radiation

Elena P. Ivanova,* The Hong Phong Nguyen, Denver P. Linklater, Phuc H. Le, Zoltan Vilagosh, Palalle G. Tharushi Perera, Dominique R. T. Appadoo, Jitraporn Vongsvivut, Tanavi Sharma, Michael G. Leeming, Nicholas A. Williamson, Eric Hanssen, Chaitali Dekiwadia, Mark J. Tobin, Saulius Juodkazis, and Rodney J. Croft

Cite This: *ACS Omega* 2024, 9, 49878−49886

Read Online

ACCESS | Metrics & More | Article Recommendations | Supporting Information

ABSTRACT: The biological effects of electromagnetic field (EMF) irradiation in the terahertz (THz) range remain ambiguous, despite numerous studies that have been conducted. In this paper, the metabolic response of *Escherichia coli* K 12 to EMF irradiation was examined using a 1.0 W m^{-2} incident synchrotron source (SS) in the range of 0.5−18.0 THz for over 90 min of continuous exposure at 25 °C. This continuous SS THz exposure induced periodic decreases in the cell growth after 10, 20, and 40 min of exposure compared to a time-matched control; however, the number of viable cells thereafter grew. The physiological status of treated cells immediately after exposure was assessed by using the direct plate counting technique and electron microscopy. Analysis of scanning electron microscopy (SEM) and high-resolution cryogenic transmission electron (cryo-TEM) micrographs showed that approximately 20% of the SS THz-exposed *E. coli* cells exhibited a deformed outer membrane, membrane perturbations, and leakage of cytosol. The proteome changes in *E. coli* cells after 18 h postexposure were associated with cellular response to plasma membrane regulation including phospholipid biosynthetic process and osmotic stress. The results of this study highlighted that *E. coli* cells can promptly activate the fundamental mechanisms in response to prolonged exposure to THz radiation that are evolutionarily developed to withstand other environmental stressors.

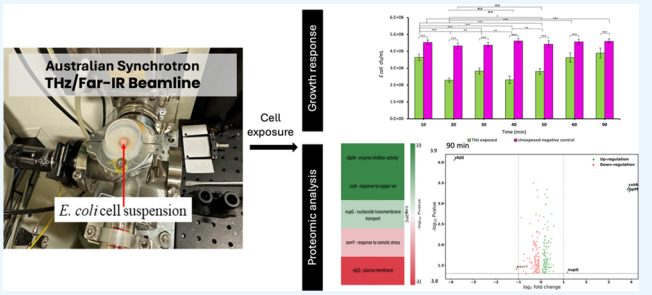

1. INTRODUCTION

The terahertz (THz) region of the electromagnetic spectrum falls between microwave and infrared wavelengths[1] (wavelength of 3.0 to 0.015 mm and photon energies of 0.413 to 82.6 meV).[2] THz radiation from solar or other cosmic sources is effectively blocked by the Earth's atmosphere so that the main source of electromagnetic field (EMF) at the THz frequencies in the natural environment is blackbody radiation (BBR) from the terrestrial environment.[3]

Over the last few decades, intensive research efforts have realized the potential applications of EMF in the THz range in biotechnology, medicine, and material science, particularly THz spectroscopy and THz imaging.[4−11] For example, THz in-line digital holography, THz near-field imaging modality, and THz endoscope prototypes have been utilized to identify abnormal tissues faster and more accurately. However, the biological effects of the THz EMF remain poorly understood. THz can penetrate various materials, such as oils, plastics, textiles, and paper. Water has a high absorption coefficient in the THz range, in the order of 160 cm^{-1} at 2.0 THz, rising to 3200 cm^{-1} at 18 THz.[12] Due to this water absorption property, the biological effects of THz radiation can be investigated in water-dominated biological systems.[4−11]

We recently showed that bacterial membranes can be transiently permeabilised by EMF of 18 GHz, leading to the uptake of nano- and genetic material for bacterial transformation without compromising cell viability.[4] However, few studies have been conducted on the effects of EMF at THz frequencies on bacteria.[13−16] It was reported that exposure to THz EMF elicited specific responses in bacteria, such as *E. coli*, including altered gene expression patterns or/and cellular morphology,[13−16] and that exposure to 1.25−3.75 THz for 15 min led to disrupted structural organization of the envelope of dividing *E. coli* cells, leading to impaired initial stages of division. Nevertheless, the effects of prolonged exposure to THz radiation on bacterial cells need further exploration.

Gaining further insight into the underlying processes involved in *E. coli* responses to THz radiation will provide

Received: September 22, 2024
Revised: November 7, 2024
Accepted: November 15, 2024
Published: December 5, 2024

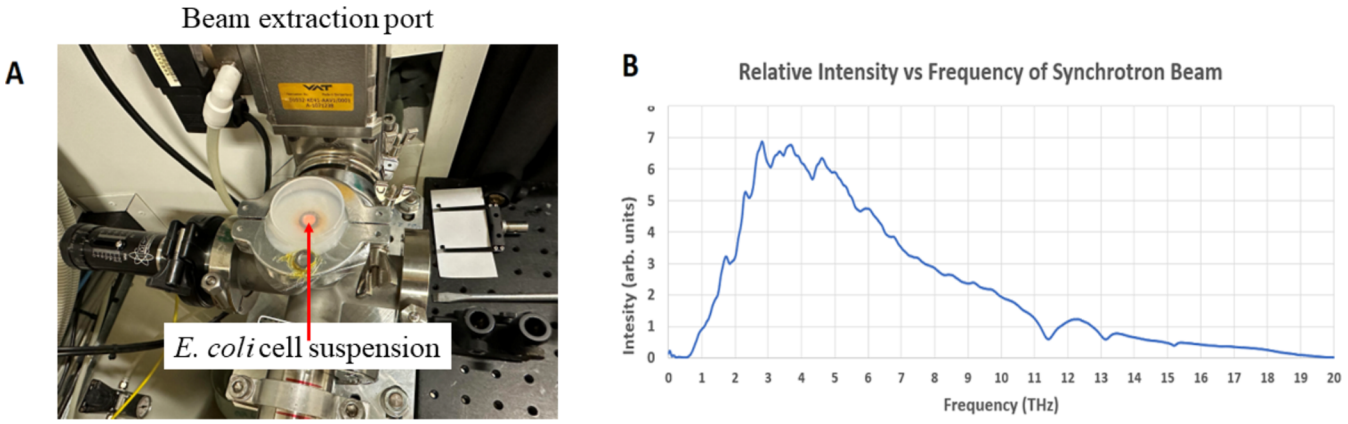

Figure 1. Experimental configurations employed at the Australian Synchrotron's THz/Far-IR beamline. (A) The setup for exposure at the BEP with the beam diameter of 4.5 mm. (B) Graphical representation of the intensity spectrum of the Australian Synchrotron's THz/Far-IR beamline, as captured by the resident Si bolometer. Intensity values are rendered in arbitrary units for THz frequencies.

fundamental knowledge regarding bacterial resilience and adaptation to EMF radiation and offer new guidelines for THz application in biotechnology, molecular biology, and genetics. Specifically, the study of bacterial stress response pathways may contribute to a deeper understanding of their adaptive mechanisms. Understanding bacterial resilience to EMF radiation may inform strategies for combating pathogenic bacteria that exhibit increased resistance to conventional treatments, particularly in the context of rising antibiotic resistance. Furthermore, by elucidating the physiological and metabolic responses of *E. coli* to THz radiation, this study also provides insight toward potential strategies for use of HF EME to mediate drug delivery and genetic transformation and provides specific information on the safety of THz wavelengths to be used in medical imaging, e.g., gastrointestinal endoscopy where bacteria would be exposed to the THz radiation emitted by an endoscopic probe. Thus, in this study, we aimed to explore the response of *E. coli* bacterial cells to increasing durations of exposure (up to 90 min) to SS 0.5 to 18.0 THz radiation using scanning electron microscopy (SEM), cryo-transmission electron microscopy (TEM), and functional proteomics analyses.

2. RESULTS

2.1. Exposure of *E. coli* Cells to SS THz Radiation. *E. coli* cells were exposed to up to 90 min of EMF (samples were collected at 10 min intervals) in the THz range using the Far THz/Far-IR beamline at the Australian Synchrotron (Clayton, Victoria, Australia). Since the penetration depth of THz radiation in water at 5 THz is 9 μm and only 4 μm at 15 THz, a single monolayer of bacterial cells was required to ensure that all cells received equal exposure (Figure 1, Sections 5 and 5.2). The cells were placed at the beam extraction port (BEP), to maximize the beam intensity since the spectrometer is not using 50% of the light (as shown in Figure 1A). The intensity energy distribution of the THz beam is shown in Figure 1B.

2.2. *E. coli* Bacterial Cell Viability in Response to Increasing Duration of Exposure to SS THz Radiation. Following the first 10 min of irradiation by SS THz beam, analysis of cell viability by the standard plate counting technique revealed that the number of viable cells declined by 19.6, ± 4.2% ($p < 0.05$) compared to the nonirradiated control. The proportion of viable cells further decreased by 48.5, ± 2.8% ($p < 0.05$) after 20 min, then increased incrementally after 30 min and decreased again after 40 min of exposure; however, the viable cell number continued to grow for the following 50 min (Figure 2).

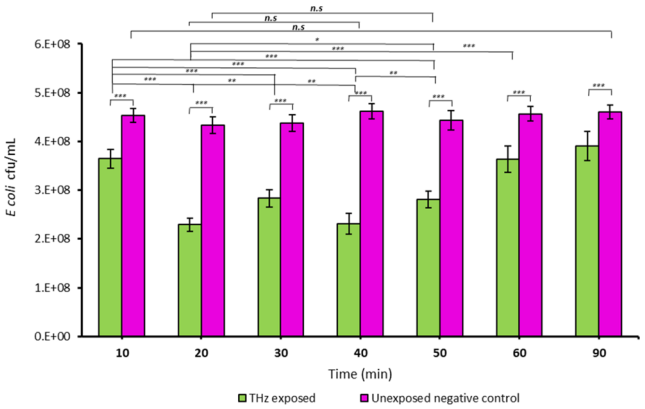

Figure 2. Growth response of *E. coli* cells to exposure to SS THz frequencies. *E. coli* cell viability was monitored over 90 at 10 min time intervals. In the untreated control group, the cells maintained their viability over 90 min. Periodic decreases and increases in the cell growth were observed during 40 min of exposure, and thereafter the number of viable cells continued to grow. * indicates a statistically significant difference as determined by two-tailed *t* test. *** $p \leq 6.30 \times 10^{-11}$; ** $p \leq 0.000001$; ns = nonsignificant, $n = 3$.

Notably, while the periodic fluctuation in cell growth as a result of EMF exposure to SS THz frequencies was not previously reported, we observed a similar fluctuation of growth of the cells of *Staphylococcus aureus* CIP 65.8^T and ATCC 25923 after multiple exposures to EMF at 18 GHz.[17]

2.3. *E. coli* Morphology. Cellular morphological changes were investigated using both SEM and cryo-TEM. The changes are shown in the micrographs in Figure 3. The cells after 10 min of EMF exposure exhibited a dehydrated appearance, accompanied by cytosolic leakages. Gram-negative bacterial cell walls are composed of two bilayered-phospholipid membranes that are separated by a periplasmic space and a peptidoglycan layer.[18] Here, we observed discernible defects in the bacterial cell wall of the EMF-exposed cells with separation of the cell envelope, as was evident in many cells. The contraction of the inner membrane on both poles of the cell was frequently observed.

https://doi.org/10.1021/acsomega.4c08710
ACS Omega 2024, 9, 49878−49886

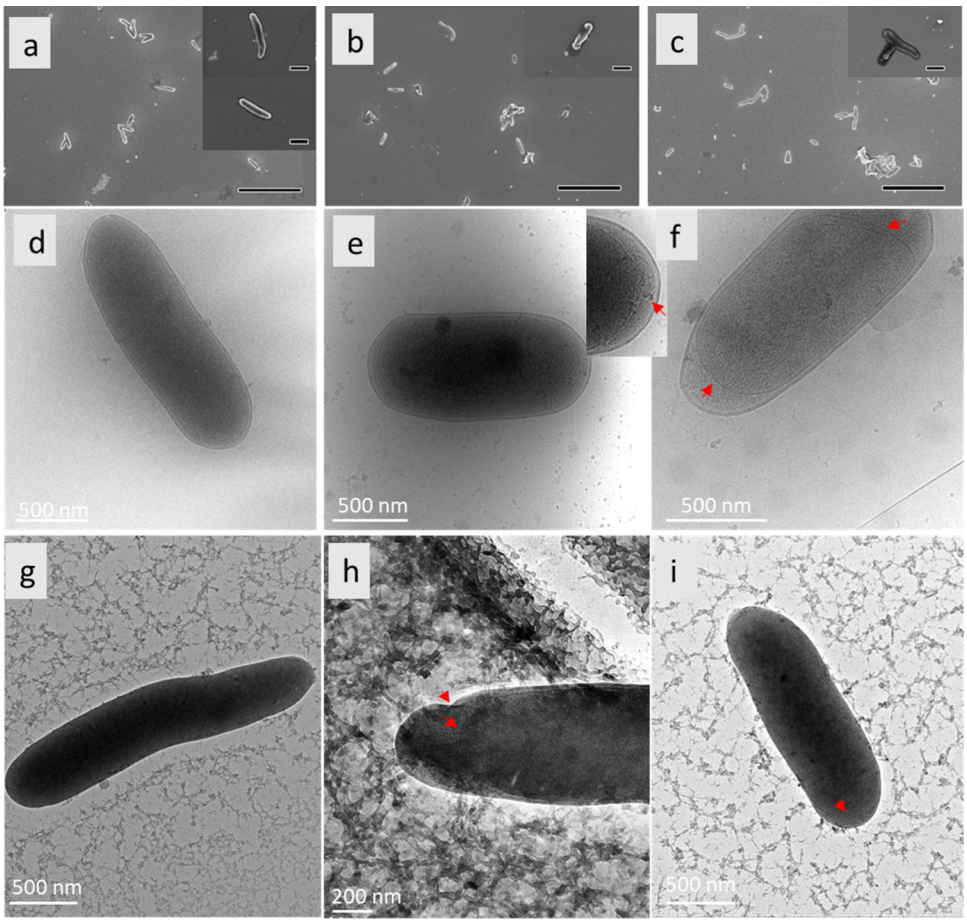

Figure 3. Morphology of *E. coli* cells in response to exposure to SS THz radiation. (a–c) SEM micrographs of *E. coli* following (a) 10 min, (b) 30 min, and (c) 90 min SS THz exposure. Following 10 min of SS THz exposure, *E. coli* cells exhibited a dehydrated appearance, accompanied by cytosolic leakages, as evidenced in the upper inset (a). At 30 and 90 min of SS THz exposure, *E. coli* cells had altered morphology as shown in (b, c), respectively. (d–h) The cryo-TEM micrographs show (d) nonexposed *E. coli* cells and (e, f) THz-exposed cells. There is a clear separation between the inner and outer cell membranes of bacteria exposed to 10 min of SS THz (red arrows, (f)). The inset image shows the bulging of the cytoplasmic material out of the inner membrane into the periplasmic space (red arrow). (g, h) Cells exposed for 90 min featuring a deformed outer membrane (OM), with a less clear demarcation between the inner and OM, encapsulated by cytosolic leakage. Red arrows highlight areas of membrane perturbation or breakage (in the case of the inner membrane). (i) Cell exposed for 90 min with a healthy bacterial morphology. Scale bars in SEM images are 10 μm, and inset scale bars are 1 μm.

The 30 and 90 min of SS EMF exposure samples also exhibited altered cells' morphology and cytosolic leakage (Figure 3). In the 30 min exposure sample, cell defects are manifested as areas of compromised integrity within the cell membrane, resulting in the perceptible leakage of cytosolic fluid. In the cryoTEM images of bacterial cells exposed to 30 min of THz radiation, the cells are surrounded by fractal arrangement of organic matter, possibly indicative of the cell debris. The release of cytosolic fluid could signify cell membrane permeability alterations induced by the THz. The cells in the nonexposed control samples did not exhibit the morphological changes. SEM images of unexposed *E. coli* cells are included in the Supporting Information, Figure S1.

Our finding of abnormal cell morphology agrees with the observations by Peltek et al., who reported that exposure to THz radiation (1.25–3.75 THz) for 15 min led to disrupted structural organization of the envelope of dividing *E. coli* cells.[16] However, they also noted the accumulation of long rod-like cells, which was not evident from our EM analyses.

2.4. Proteomic Analysis of *E. coli* Cells after 18 h Postexposure to SS THz Radiation. Since the SS THz-induced changes in bacterial growth were notable at 10, 30, and 90 min, these time intervals were selected for detailed proteomics analysis. Exposed cells were grown for 18 h in optimal growth conditions before being collected to analyze their metabolic status. Proteomics analysis of *E. coli* cells after 18 h postexposure to EMF showed alterations in the expression levels of 461, 271, and 230 proteins at 10, 30, and 90 min of exposure, respectively, compared to the nonexposed control group. However, when we applied a threshold of *p-value* = 0.05 and a fold change (FC) of 2 (Log2 FC = 1) or more, there was only 1 differentially expressed protein at 10 min, 15 proteins at 30 min, and 5 proteins at 90 min. The differentially expressed proteins are included in the Supporting Information, Table S1, and are discussed below.

2.4.1. Analysis of Changes in Cellular Biological Processes after 10 min Exposure to SS THz Radiation. Following 10 min of SS THz exposure, the postexposure bacterial proteome was primarily unchanged, but we observed the upregulation of a single protein (gene promoter *yahoo*) that encodes a ferritin-like periplasmic protein.

2.4.2. Analysis of Changes in Cellular Biological Processes at after 30 min Exposure to SS THz Radiation. The cells

https://doi.org/10.1021/acsomega.4c08710
ACS Omega 2024, 9, 49878–49886

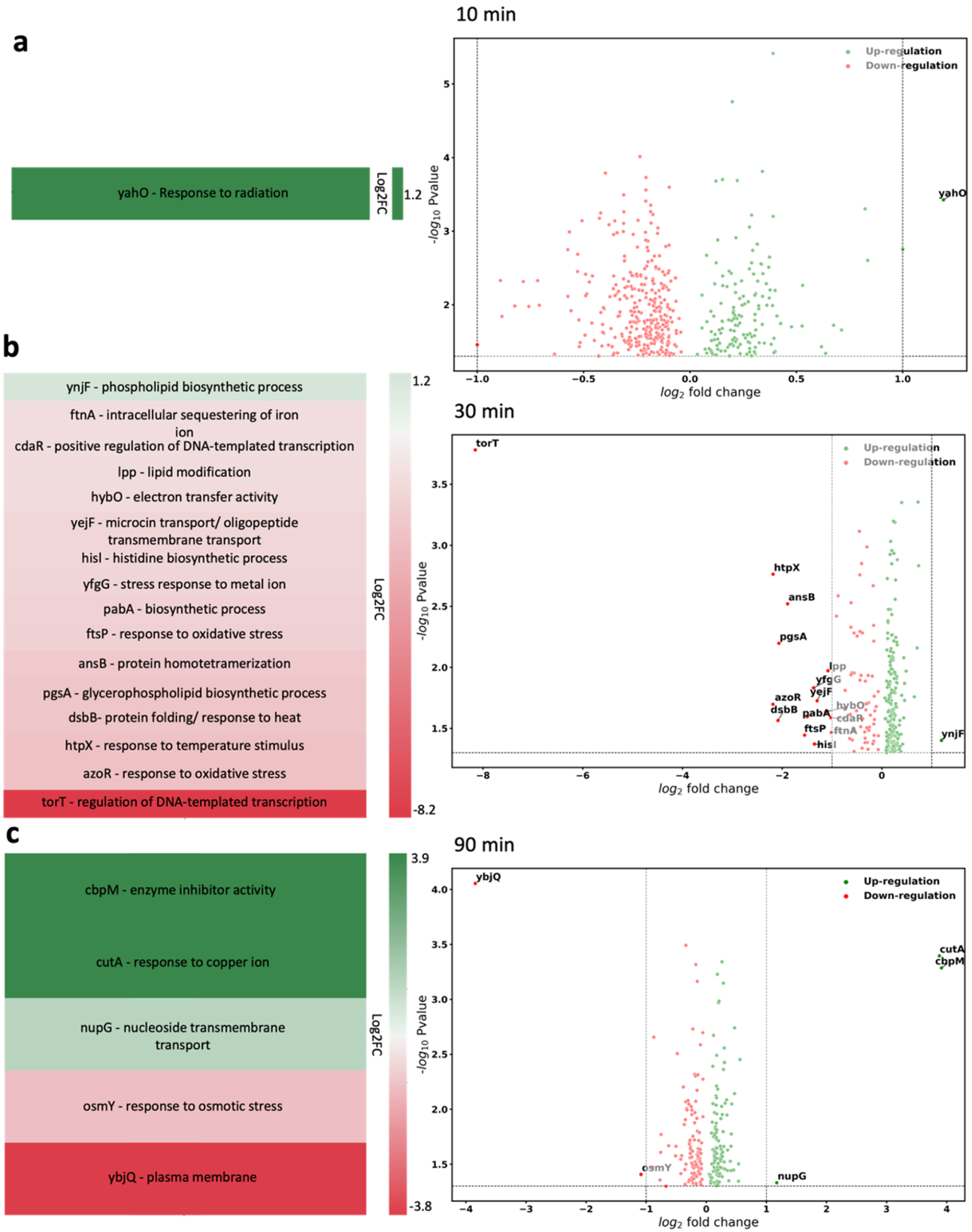

Figure 4. Proteomics analysis of *E. coli* bacteria after 18 h postexposure to SS THz radiation. Heatmap of the main biological processes altered through exposure to SS THz radiation and corresponding volcano plot showing the significance of differential expression of promotor genes vs log2 fold change of upregulated and downregulated genes for bacteria exposed to THz EMF for (a) 10 min, (b) 30 min, and (c) 90 min. Green and red colors represent upregulated and downregulated proteins, respectively. Brighter shades of green and red indicate higher fold changes, where their | log2 fold changel are greater than 1.

https://doi.org/10.1021/acsomega.4c08710
ACS Omega 2024, 9, 49878−49886

exposed to SS THz radiation for 30 min exhibited 15 proteins whose expression was downregulated, and one protein, *ynjF*, inner membrane protein, member of CDP-alcohol phosphatidyl transferase family, which is involved in phospholipid biosynthetic process, was upregulated. The 16 proteins are listed in Figure 4b.

The majority of identified downregulated proteins form part of the cell membrane componentry, e.g., *Lpp*, major outer membrane lipoprotein, *ftsP*, a septal ring component that is required for growth during stress, or cell response to oxidative stress, e.g., *azoR, flsP*.[19] One gene, *TorT*, is a periplasmic sensory protein associated with anaerobic respiration, and regulation of DNA-templated transcription via the TorRS two-component regulatory system was notably downregulated, with a log2 FC of 8 (Figure 4b). We hypothesize that the downregulation of those proteins responsible for cell protection during exposure to environmental stressors might occur as a result of the cells returning to a nonstress environment. An increased expression for *ynjF* gene may suggest ongoing postexposure cell membrane reparations.

2.4.3. Analysis of Changes in Cellular Biological Processes after 18 h Postexposure to 90 min to SS THz Radiation. Proteomics analysis of *E. coli* cells after 18 h postexposure suggested the changes in 5 specific genes: upregulation of *cutA*, *cbpM*, and *nupG* and downregulation of *ybjQ* and *osmY*.

The upregulated genes appeared being involve in DNA synthesis processes, e.g., *cbpM* is part of the protein family, which modulates the activity of the DnaK chaperone system; *cutA* is a divalent-cation tolerance protein and *nupG* is a nucleoside transporter with broad-specificity transporter of purine and pyrimidine nucleosides.

Two downregulated proteins, *osmY*, accountable for response to osmotic stress, and *ybjQ*, responsible for metabolic regulation of plasma membrane,[20] are signaling the completion of cell recovery after 90 min.

3. DISCUSSION

E. coli bacteria serve as a valuable model organism for investigating bacterial physiology, genetics, and cellular responses to environmental stimuli.[21−24] Its adaptability to a wide range of conditions has been underscored by a multitude of studies, highlighting its resilience mechanisms that enable survival and propagation across diverse ecological niches.[21−23,25,26] While extensive research has been dedicated to elucidating *E. coli* cells' responses to conventional stressors such as temperature variations, pH fluctuations and oxidative stress,[21−23,25,26] less research effort has focused on investigating unconventional stressors, including THz radiation.[13−15]

In this work, we explored the proteomics changes in *E. coli* bacteria after 18 h of postexposure to SS 0.5−18 THz radiation. Functional proteomics analysis of the downregulated proteins in *E. coli* cells after 30 and 90 min of THz exposure indicated that these proteins are involved in maintaining the integrity and permeability of the outer and inner membranes, as well as in stress response and membrane repair processes. During THz exposure, these proteins might be activated to help the cells cope with stress. However, they are downregulated during the recovery stage because they are no longer needed. Indeed, it has been observed that exposure to nonthermal terahertz radiation activated *E. coli* gene networks related to oxidative stress and copper ion homeostasis but does not affect those induced by antibiotics, protonophores, or superoxide anions.[14,26] For example, after irradiating *E. coli* strain JM109 cells using SS 2.3 THz irradiation for 15−30 min, there were identified seven transcription factor TF genes significantly overexpressed (log2 fold change $\geq$ 1, $P < 0.05$) under THz irradiation: cadC, caiF, chbR, gadW, matA, tdcR, and ydeO. Later, THz-sensitive inducible promoters were used to identify genetically modified biosensor *E. coli* cells expressing fluorescence under THz irradiation. The authors showed that transcription factors katG, copA, tcdR, safA, chbB, and matA were all activated by THz stimulus.[14,15,27−30] Similarly, Peltek et al. observed that there was differential expression of genes of transcription factors related to the regulation of cell aggregation processes, genes of chaperone-usher fimbria biogenesis, genes of curli amyloid fibril biogenesis, genes of colanic acid biosynthesis, and genes related to cell division.[31] Electron microscopy revealed invaginations of the cell envelope and breaches of the cell membrane. The irradiated bacteria underwent increased aggregation, potentially as a result of changes in the adhesive properties of the pili. There were aberrations in the cell wall structure that were purported to impair the cell at the initial stages of division and resulted in accumulation of long rod-like cells.[31] In our study, there was no accumulation of long, rod-like cells, suggesting that DNA replication and cell division was successfully accomplished by majority "THz-exposed cells."

In another study, THz irradiation negatively affected the overall metabolism and growth of *Geobacillus icigianus* cells, e.g., through a decrease in translation efficiency and in the activity of the respiratory system as well as in the synthesis of peptidoglycan and of cofactors NADH, FAD, and pyridoxal 50-phosphate. When *G. icigianus* bacteria were allowed to recover postexposure to 1.0−1.4 THz at 1.0−1.4 mW/cm^2 for 6 h, it was found that the cellular systems relating to stress defense, chemotaxis, and, partially, cell growth were restored, but the respiration and energy metabolism, biosynthesis of riboflavin, cofactors, peptidoglycan, and translation system components remained affected.[32] Furthermore, the antiproliferative effects of THz radiation toward the yeast *Saccrymyces cerevisiae* was elicited by 0.105 THz of power density of 0.83 $\pm$ 0.02 mW/cm^2.[33] It was recently reported that reactive oxygen species (ROS) produced by THz radiation at low concentrations were toxic to human cells[34] and may affect bacterial cells viability. ROS generation was also involved in increased membrane permeability.[35] However, in this study, the proteomics analysis of *E. coli* cells after postprolonged exposure to THz radiation under current experimental setup did not reveal any down- (or up) regulated genes associated with ROS generation.

Herein, broadband, continuous wave SS THz radiation incurred a cyclical decrease and then increase in the proliferative capacity of *E. coli*. We observed a periodic decrease and increase in viable cell number. Electron microscopy analysis confirmed the appearance of cells with deformed outer membranes, membrane perturbation, and cytosol leakage. However, considering the very small difference in absolute viable bacteria numbers in Figure 2 between treated and nontreated bacteria, it is unlikely that the bacteria we observed by SEM and cryoTEM remained nonviable. The ability of the bacteria to remain viable even after THz treatment and observed membrane damage was analyzed by functional proteomics. Indeed, proteomic analyses of post-exposed cells returned to a nonstress environment confirmed the downregulation of genes involved in the cellular stress response and membrane repair processes. Following 10 min of SS THz exposure, the postexposure bacterial proteome was

https://doi.org/10.1021/acsomega.4c08710
ACS Omega 2024, 9, 49878−49886

primarily unchanged, but we observed the upregulation of a single ferritin-like periplasmic protein that is involved in cell response to radiation. By contrast, postexposure to 30 min of THz radiation, one inner membrane protein that is involved in phospholipid biosynthetic process was upregulated, and 15 proteins that mostly form part of the cell membrane componentry were downregulated. Finally, postexposure to 90 min of THz radiation, the upregulated genes appeared being involve in DNA synthesis processes while the + expression of proteins involved in response to osmotic stress and metabolic regulation of plasma membrane[20] was down-regulated. Therefore, we hypothesize that the antiproliferative effects and membrane perturbation of *E. coli* induced by THz radiation observed in this study were promptly repaired through activation of the adaptive physiological responses to stress and did not lead to long-term detrimental effects to the bacteria.

4. CONCLUSIONS

In our study of the effects of prolonged exposure to SS THz radiation on *E. coli* cells, we observed a periodic decrease and increase in the viable cell number over 90 min of exposure. Analysis of SEM and high-resolution cryo-TEM micrographs showed that some SS THz-exposed *E. coli* cells exhibited a deformed outer membrane, membrane perturbations, and leakage of cytosol. However, functional proteomic analysis of *E. coli* cells after 18 h postexposure revealed that *E. coli* cells effectively activated cellular responses to osmotic stress, plasma membrane regulation, and phospholipid biosynthetic process. Therefore, *E. coli* cells do not suffer long-term detriments from exposure to millimeter waves but can promptly activate the adaptive physiological responses to withstand THz radiation that are evolutionarily developed to withstand other environmental stressors. These data further inform the safety of the application of mm-wave HF EMF in biological systems. Indeed, understanding of the key physiological and metabolic response of cells to prolonged THz radiation provides foundation for the informed use of THz imaging modalities.

5. MATERIALS AND METHODS

5.1. Cell Growth Conditions and Sample Preparation. *E. coli* K 12/JM109 was purchased from Promega (NSW, Australia). Pure culture was stored at −80 °C in Luria−Bertani broth (LB) (Oxoid) supplemented with 20% (v/v) glycerol. The bacteria were thawed from −80 °C and were revived on LB agar (LB) (Oxoid) for 24 h at 37 °C before THz exposure. For each independent experiment, fresh working bacterial suspensions were prepared by inoculating several colonies in 10 mM phosphate-buffered saline (PBS; pH 7.4), and the cell density was adjusted to 4×10^8 CFU per mL (optical density at 600 nm [OD_{600}] = 0.18) using a NanoDrop 2000/2000c spectrophotometer (ThermoFisher Scientific, Australia).

5.2. Exposure of *E. coli* Cells to SS THz Radiation. *E. coli* cells suspension (approximately 5.17×10^6 cells) was used to ensure that on a thin polyethylene film with a radius of 2.5 mm (yielding a surface area of approximately 17.2 mm^2), each cell would have sufficient surface area during exposure to the THz beam. The monolayer was constructed by pipetting 35 μL of freshly prepared working bacterial suspension into the O-ring, sealed with grease on a polyethylene (PE) film (12 μm thick). The *E. coli* cells, being approximately 1.0−2.0 μm long with a radius of about 0.5 μm, received a reasonably uniform exposure profile equivalent to a sample depth of 5 μm. The cells were decanted into individual sample holders for each period and exposed to THz radiation for durations of 10, 20, 30, 40, 50, 60, and 90 min. A fresh sample was used for every exposure duration, and each sample had a control assigned. The control samples were held in identical holders and placed next to the exposed sample, out of the path of the beam but subjected to identical conditions in every other manner.

The cells were placed at the beam extraction port (BEP) to maximize the beam intensity as shown in Figure 1A. The spectrum of the THz beam is shown in Figure 1B. The configuration of the Australian Synchrotron's THz beam delivered energies approaching 0.058 mW over a 4.5 mm diameter spot size, giving a total intensity of ∼1.25 Wm^{2-} (0.125 mW cm^{-2}) at the BEP. After adjustments for the losses due to the sample holder, the intensity was reduced to 1.0 W m^{-2}. The maximum beam intensity was centered on 4.0 THz with the half-maximum points occurring at 2.0 THz and 8.0 THz, with a long THz tail in the region to 18.0 THz. The beam operates at a frequency of 500 MHz, with a pulse duration 0.23 ns, giving a pulse length of 7 cm. Assuming a Gaussian form, the maximum intensity of the beam is on the order of 20 W m^{-2} delivered over 4 ns. The peak of the radiation intensity is equivalent to that of visible light on an overcast day.

The temperature of the sample was recorded every 10 min during each exposure using an IR thermometer. The estimated total energy delivered to the cells over the exposure times is presented in Table 1. The average temperature during THz exposure was 24.57 ± 0.12 °C, with a negligible increase of 0.12 °C.

Table 1. Estimated Energy Delivered to the Sample over the Increasing Exposure Times

time (min)	energy (Jm^{-2})	energy (mJ, total)	energy (mJ μL^{-1})
10	600	10.5	0.30
20	1200	21	0.60
30	1800	31.5	0.90
40	2400	42	1.20
50	3000	52.5	1.50
60	3600	63	1.80
90	5400	94.5	2.70

5.3. Cell Viability Assay. The quantification of viable cells (colony-forming units, cfu) at each time interval (10, 20, 30, 40, 50, 60, and 90 min) was conducted by performing a 6-fold serial dilution and plating 100 μL of diluted cell suspensions on solidified nutrient agar plates (NA, Oxoid Ltd., Basingstoke, Hampshire, England) immediately after SS THz exposures and in parallel with those of the control samples. Five plates for each time interval and condition (exposed and nonexposed samples) were spread-plated and incubated for 24 h at 37 °C. Following incubation, CFU were counted. Three independent technical replicates were carried out. Statistical significance was determined using a two-tailed Student's *t* test.

5.4. Scanning Electron Microscopy (SEM). For a visual examination of cell morphology, *E. coli* cells were fixed in 2.5% glutaraldehyde for 35 min. Samples were then dehydrated in a graded ethanol series of 30, 50, 70, 90, and 100% (×2) for 15 min each and finally sputter-coated with 10 nm of Iridium. SEM images were obtained using a FEI Verios 460L XHR

https://doi.org/10.1021/acsomega.4c08710
ACS Omega 2024, 9, 49878−49886

SEM under a high vacuum at an accelerating voltage of 3 kV. A through-the-lens detector (TLD) was used for imaging.

5.5. Cryogenic Transmission Electron Microscopy (cryoTEM). CryoTEM was also employed to confirm the cell morphology. Briefly, 2.5 μL of collected *E. coli* cells was applied to a glow-discharged carbon grid, blotted twice at the back for 15 s and once at the front for 4 s. The cells were then vitrified, mounted into a Gatan cryoholder (Gatan, Inc., Pleasanton, CA), and stored in cold liquid nitrogen for analysis. Images of *E. coli* cells were acquired using a 300 kV Tecnai G2 F30 system (FEI, Eindhoven, The Netherlands). A minimum of 15 fields of view were recorded per sample.

5.6. Proteomic Analysis of *E. coli* Cells Exposed to SS THz Radiation. The proteomics data of the *E. coli* cells exposed to SS THz radiation were generated using liquid chromatography coupled to tandem mass spectrometry (LC-MS/MS)-based proteomic workflow.

5.6.1. Protein Extraction. Cell pellets were suspended in 5% w/v sodium dodecyl sulfate (SDS) (Merck, Australia) in 100 mM triethylammonium bicarbonate (TEAB) (Merck, Australia), vortexed, and sonicated for 20 min. Afterward, the suspension was centrifuged at 13,000*g* for 8 min to pellet any remaining insoluble components. Then, the supernatant was transferred to a new Eppendorf tube. BCA assay (Pierce BCA Protein Assay kit, ThermoFisher Scientific) was performed to estimate the protein concentration. 50 μg of proteins from each sample was taken

Reduction and alkylation were performed using 10 mM tris(2-carboxyethyl)phosphine (TCEP) (BondBreaker, ThermoFisher Scientific) at 55 °C for 15 min and 50 mM iodoacetamide (IAA) (Sigma) at RT in dark conditions for 45 min. The SDS solution was then acidified with 1.2% (v/v) phosphoric acid (Merck, Australia). The acidified solution was mixed with S-trap binding buffer (100 mM TEAB in 90% v/v HPLC grade MeOH) to create a colloidal protein suspension. The samples were loaded onto the S-trap microcolumns and centrifuged at 4000*g* for 30 s, trapping the proteins in the S-trap column matrix. The trapped proteins were washed 4 times with 150 μL of S-trap binding buffer with centrifugation at 4000*g* for 30 s between each wash. Protein digestion was performed by Pierce Trypsin Protease (ThermoFisher Scientific) (50 mM TEAB containing a 1:50 w/w ratio of trypsin to protein) and incubated overnight at 37 °C.

Peptides were separated using a sequence of elution solutions, which consisted of TEAB (50 mM), 0.2% formic acid, and 50% acetonitrile (ACN) (Merck, Australia). The eluted peptides were then pooled together and dried using SpeedVac concentrator (ThermoFisher Scientific).The dried peptides were stored at −80 °C until further analysis.

5.6.2. LC-MS/MS Analysis. Peptides were reconstituted in 0.1% (v/v) TFA and 2% (v/v) ACN for LC−MS/MS analysis on an Orbitrap Eclipse mass spectrometer (Thermo Scientific) equipped with a nanoflow reversed-phase-HPLC (Ultimate 3000 RSLC, Dionex). Peptides were injected onto the Acclaim Pepmap nanotrap column (Dinoex-C18, 100 Å, 75 μm × 2 cm) at an isocratic flow of 5 μL/min of 2% v/v CH_3CN containing 0.1% v/v formic acid for 6 min applied before the enrichment column was switched in-line with the analytical column (Acclaim Pepmap RSLC analytical column) (Dinoex-C18, 100 Å, 75 μm × 50 cm).

The eluents were 5% DMSO in 0.1% (v/v) formic acid (solvent A) and 5% DMSO in 100% (v/v) CH_3CN and 0.1% (v/v) formic acid (solvent B). The flow gradient was (i) 0−6 min at 3% B, (ii) 6−95 min, 3−23% B, (iii) 95−105 min, 23−40% B, (iv) 105−110 min, 40−80% B, (v) 110−115 min, 80−80% B, (vi) 115−115.1 min, 80−3% and equilibrated at 3% B for 10 min before the next sample injection. Data were acquired in a data dependent mode (DDA). All spectra were acquired in positive ionization mode with full scan MS acquired from m/z 375−1500 in the FT mode at a mass resolving power of 120,000, after accumulating to an AGC target value of 4.0E5, with a maximum accumulation time of 50 ms. For MS/MS, most intense precursor ions are selected using a top speed acquisition mode where precursors having charge states 2−7 are selected using a 3 s scan method, at a normalized AGC target of 100%, automatic injection, a normalized collision energy of 30%, and spectra acquired at a resolving power of 15,000. Dynamic exclusion was used for 30 s.

5.6.3. Data Processing and Analysis. Raw files are searched using MaxQuant v2.4.8.0 (developed by Max Planck Institute of Biochemistry, Germany) against the Human database Uniprot. Search parameters were trypsin as the enzyme, missed cleavage 2, acetylation at the protein N-terminal and oxidation at methionine as variable modification, and carbamidomethyl at cysteine as fixed modification. A 1% false discovery rate (FDR) at PSM, peptide, and protein levels was selected. The protein abundance data from MaxQuant were analyzed using Perseus (v1.6.15.0).

Perseus v1.6.15.0 (developed by Max Planck Institute of Biochemistry, Germany) was used for unsupervised hierarchical clustering analysis (HCA). The missing value from the data set was imputed using the "Replacing missing value from normal distribution" in Perseus. Two sample tests were performed for assessing the statistical significance between groups ($p \leq 0.05$). Proteins that qualified for log2-fold change ≥ 1 or ≤ -1 and were statistically significant ($p \leq 0.05$) were considered differentially regulated. The protein functional annotations including biological processes and molecular functions were analyzed using GeneCodis4.[36]

Statistical analysis was conducted to assess differences in the respective abundances of proteins. An unpaired Student's *t* test was utilized, and multiple (ten) comparisons were corrected using the Holm-Šidák method. Volcano plots were generated, and the statistical significance was determined using GraphPad Prism 9.1.2.

■ ASSOCIATED CONTENT

Supporting Information

The Supporting Information is available free of charge at https://pubs.acs.org/doi/10.1021/acsomega.4c08710.

Proteins significantly expressed by *E. coli* cells exposed to SS THz radiation for 10, 30, and 90 min (Table S1); morphology of *E. coli* cells that were not exposed to SS THz radiation (Figure S1) (PDF)

■ AUTHOR INFORMATION

Corresponding Author

Elena P. Ivanova − *STEM College, School of Science, RMIT University, Melbourne, Victoria 3000, Australia;*
orcid.org/0000-0002-5509-8071;
Email: elena.ivanova@rmit.edu.au

https://doi.org/10.1021/acsomega.4c08710
ACS Omega 2024, 9, 49878−49886

Authors

The Hong Phong Nguyen − *STEM College, School of Science, RMIT University, Melbourne, Victoria 3000, Australia*

Denver P. Linklater − *Biomedical Engineering, Graeme Clark Institute, The University of Melbourne, Parkville, Victoria 3010, Australia*

Phuc H. Le − *STEM College, School of Science, RMIT University, Melbourne, Victoria 3000, Australia; Ian Holmes Imaging Centre, ARC Centre for Cryo Electron Microscopy of Membrane Protein and Department of Biochemistry and Pharmacology, Bio21 Institute, University of Melbourne, Parkville, Victoria 3052, Australia;* orcid.org/0000-0003-2910-7509

Zoltan Vilagosh − *STEM College, School of Science, RMIT University, Melbourne, Victoria 3000, Australia*

Palalle G. Tharushi Perera − *STEM College, School of Science, RMIT University, Melbourne, Victoria 3000, Australia;* orcid.org/0000-0002-2787-9938

Dominique R. T. Appadoo − *THz/Far-IR Beamline, ANSTO−Australian Synchrotron, Clayton, Victoria 3168, Australia*

Jitraporn Vongsvivut − *THz/Far-IR Beamline, ANSTO−Australian Synchrotron, Clayton, Victoria 3168, Australia*

Tanavi Sharma − *Melbourne Mass Spectrometry and Proteomics Facility, Bio 21 Molecular Science and Biotechnology Institute, University of Melbourne, Parkville, Victoria 3010, Australia*

Michael G. Leeming − *Melbourne Mass Spectrometry and Proteomics Facility, Bio 21 Molecular Science and Biotechnology Institute, University of Melbourne, Parkville, Victoria 3010, Australia*

Nicholas A. Williamson − *Melbourne Mass Spectrometry and Proteomics Facility, Bio 21 Molecular Science and Biotechnology Institute, University of Melbourne, Parkville, Victoria 3010, Australia*

Eric Hanssen − *Ian Holmes Imaging Centre, ARC Centre for Cryo Electron Microscopy of Membrane Protein and Department of Biochemistry and Pharmacology, Bio21 Institute, University of Melbourne, Parkville, Victoria 3052, Australia;* orcid.org/0000-0002-4064-1844

Chaitali Dekiwadia − *RMIT Microscopy and Microanalysis Facility, College of Science, Engineering and Health, RMIT University, Melbourne, Victoria 3001, Australia*

Mark J. Tobin − *THz/Far-IR Beamline, ANSTO−Australian Synchrotron, Clayton, Victoria 3168, Australia*

Saulius Juodkazis − *Centre for Quantum and Optical Sciences, Swinburne University of Technology, Hawthorn, Victoria 3122, Australia;* orcid.org/0000-0003-3542-3874

Rodney J. Croft − *School of Psychology, University of Wollongong, Wollongong, New South Wales 2522, Australia*

Complete contact information is available at: https://pubs.acs.org/10.1021/acsomega.4c08710

Author Contributions

E.P.I., T.H.P.N., D.P.L., and P.H.L. designed the experiments. T.H.P.N., D.P.L., Z.V., P.G.T.P., D.R.T.A., and J.V. performed the SS EMF experiments. D.P.L., P.H.L., T.H.P.N., and C.D. performed the SEM and TEM experiments. P.H.L., D.P.L., T.H.P.N., T.S., M.G.L., and N.A.W. performed and analyzed the proteomic experiments. D.P.L., T.H.P.N., P.H.L., and Z.V. generated the figures and wrote the original draft. E.P.I., E.H., M.J.T., S.J., and R.J.C. wrote, revised, and edited the manuscript.

Notes

The authors declare no competing financial interest.

■ ACKNOWLEDGMENTS

The authors gratefully acknowledge the RMIT Microscopy and Microanalysis Facility (RMMF), a linked laboratory of Microscopy Australia. The authors would like to acknowledge the Melbourne Mass Spectrometry and Proteomics Facility and Ian Holmes Imaging Centre at the Bio21 Molecular Science and Biotechnology Institute at The University of Melbourne. The exposure experiment was undertaken on the THz/Far-IR beamline at the Australian Synchrotron (Victoria, Australia), part of ANSTO, through merit-based beamtime proposals. The authors would like to acknowledge financial support of the NHMRC Centre of Research Excellence for Electromagnetic Bioeffects Research (Grant No. CRE1042464 and CRE1135076) and the funding received by the Australian Radiation Protection and Safety Agency (ARPANSA) under the EMF Research Framework.

■ REFERENCES

(1) Pawar, A. Y.; Sonawane, D. D.; Erande, K. B.; Derle, D. V. Terahertz technology and its applications. *Drug Invent. Today* **2013**, *5* (2), 157−163.

(2) Koenig, S.; Lopez-Diaz, D.; Antes, J.; Boes, F.; Henneberger, R.; Leuther, A.; Tessmann, A.; Schmogrow, R.; Hillerkuss, D.; Palmer, R.; et al. Wireless sub-THz communication system with high data rate. *Nat. Photonics* **2013**, *7* (12), 977−981.

(3) Zwinkels, J. C.; Ikonen, E.; Fox, N. P.; Ulm, G.; Rastello, M. L. Photometry, radiometry and 'the candela': evolution in the classical and quantum world. *Metrologia* **2010**, *47* (5), No. R15.

(4) Son, J.-H.; Oh, S. J.; Cheon, H. Potential clinical applications of terahertz radiation. *J. Appl. Phys.* **2019**, *125* (19), No. 190901, DOI: 10.1063/1.5080205.

(5) Perera, P. G. T.; Vilagosh, Z.; Linklater, D.; Nguyen, T. H. P.; Appadoo, D.; Vongsvivut, J.; Tobin, M.; Dekiwadia, C.; Croft, R.; Ivanova, E. P. Translocation and fate of nanospheres in pheochromocytoma cells following exposure to synchrotron-sourced terahertz radiation. *J. Synchrotron Radiat.* **2023**, *30* (4), 780−787.

(6) Perera, P. G. T.; Appadoo, D. R. T.; Cheeseman, S.; Wandiyanto, J. V.; Linklater, D.; Dekiwadia, C.; Truong, V. K.; Tobin, M. J.; Vongsvivut, J.; Bazaka, O.; et al. PC 12 Pheochromocytoma cell response to super high frequency terahertz radiation from synchrotron source. *Cancers* **2019**, *11* (2), No. 162.

(7) Sitnikov, D. S.; Ilina, I. V.; Pronkin, A. A.; Ovchinnikov, A. V.; Chefonov, O. V.; Zurina, I. M.; Gorkun, A. A.; Kosheleva, N. V. Studying the effect of high-power coherent terahertz pulses on mesenchymal stem cells. *J. Phys.: Conf. Ser.* **2018**, *1147* (1), No. 012060.

(8) Cocker, T. L.; Jelic, V.; Hillenbrand, R.; Hegmann, F. A. Nanoscale terahertz scanning probe microscopy. *Nat. Photonics* **2021**, *15* (8), 558−569.

(9) Zhou, R.; Wang, C.; Xu, W.; Xie, L. Biological applications of terahertz technology based on nanomaterials and nanostructures. *Nanoscale* **2019**, *11* (8), 3445−3457.

(10) Zhao, L.; Yi, R.; Liu, S.; Chi, Y.; Tan, S.; Dong, J.; Wang, H.; Zhang, J.; Wang, H.; Xu, X.; et al. Biological responses to terahertz radiation with different power density in primary hippocampal neurons. *PLoS One* **2023**, *18* (1), No. e0267064.

(11) Zhang, J.; Li, S.; Le, W. Advances of terahertz technology in neuroscience: Current status and a future perspective. *iScience* **2021**, *24* (12), No. 103548.

(12) Segelstein, D. J. *The Complex Refractive Index of Water*; Department of Physics. University of Missouri-Kansas City, 1981.

(13) Zhao, J.; Hu, E.; Shang, S.; Wu, D.; Li, P.; Zhang, P.; Tan, D.; Lu, X. Study of the effects of 3.1 THz radiation on the expression of

recombinant red fluorescent protein (RFP) in *E. coli*. *Biomed. Opt. Express* **2020**, *11* (7), 3890−3899.
(14) Peltek, S. E.; Demidova, E. V.; Popik, V. M.; Goryachkovskaya, T. N. Stress-induced systems in *Escherichia coli* and their response to terahertz radiation. *Russ. J. Genet.: Appl. Res.* **2017**, *7* (8), 858−868.
(15) Demidova, E. V.; Goryachkovskaya, T. N.; Mescheryakova, I. A.; Malup, T. K.; Semenov, A. I.; Vinokurov, N. A.; Kolchanov, N. A.; Popik, V. M.; Peltek, S. E. Impact of terahertz radiation on stress-sensitive genes of *E. coli* cell. *IEEE Trans. Terahertz Sci. Technol.* **2016**, *6* (3), 435−441.
(16) Peltek, S.; Meshcheryakova, I.; Kiseleva, E.; Oshchepkov, D.; Rozanov, A.; Serdyukov, D.; Demidov, E.; Vasiliev, G.; Vinokurov, N.; Bryanskaya, A.; et al. *E. coli* aggregation and impaired cell division after terahertz irradiation. *Sci. Rep.* **2021**, *11* (1), No. 20464.
(17) Nguyen, T. H. P.; Pham, T. H. V.; Nguyen, S. H.; Baulin, V.; Croft, R. J.; Phillips, B.; Crawford, R. J.; Ivanova, E. P. The bioeffects resulting from prokaryotic cells and yeast being exposed to an 18 GHz electromagnetic field. *PLoS One* **2016**, *11* (7), No. e0158135.
(18) Cian, M. B.; Giordano, N. P.; Mettlach, J. A.; Minor, K. E.; Dalebroux, Z. D. Separation of the cell envelope for Gram-negative bacteria into inner and outer membrane fractions with technical adjustments for *Acinetobacter baumannii*. *J. Visualized Exp.* **2020**, No. 158, No. 60517, DOI: 10.3791/60517.
(19) Esquilin-Lebron, K.; Dubrac, S.; Barras, F.; Boyd, J. M. Bacterial approaches for assembling Iron-sulfur proteins. *mBio* **2021**, *12* (6), No. e0242521.
(20) Lesniak, J.; Barton, W. A.; Nikolov, D. B. Structural and functional features of the *Escherichia coli* hydroperoxide resistance protein OsmC. *Protein Sci.* **2003**, *12* (12), 2838−2843.
(21) Bhatia, R. P.; Kirit, H. A.; Predeus, A. V.; Bollback, J. P. Transcriptomic profiling of *Escherichia coli* K-12 in response to a compendium of stressors. *Sci. Rep.* **2022**, *12* (1), No. 8788.
(22) Jozefczuk, S.; Klie, S.; Catchpole, G.; Szymanski, J.; Cuadros-Inostroza, A.; Steinhauser, D.; Selbig, J.; Willmitzer, L. Metabolomic and transcriptomic stress response of *Escherichia coli*. *Mol. Syst. Biol.* **2010**, *6*, No. 364.
(23) Gold, A.; Chen, L.; Zhu, J. More than Meets the Eye: Untargeted metabolomics and lipidomics reveal complex pathways spurred by activation of acid resistance mechanisms in *Escherichia coli*. *J. Proteome Res.* **2022**, *21* (12), 2958−2968.
(24) Kaper, J. B.; Nataro, J. P.; Mobley, H. L. T. Pathogenic *Escherichia coli*. *Nat. Rev. Microbiol.* **2004**, *2* (2), 123−140.
(25) Li, J.; Zhang, X.; Ashokkumar, M.; Liu, D.; Ding, T. Molecular regulatory mechanisms of *Escherichia coli* O157:H7 in response to ultrasonic stress revealed by proteomic analysis. *Ultrason. Sonochem.* **2020**, *61*, No. 104835.
(26) Wang, Y.; Zhou, D.; Yang, H. Metabolic Responses of "Big Six" *Escherichia coli* in wheat flour to thermal Treatment revealed by nuclear magnetic resonance spectroscopy. *Appl. Environ. Microbiol.* **2022**, *88* (7), No. e0009822.
(27) Demidova, E. V.; Goryachkovskaya, T. N.; Malup, T. K.; Bannikova, S. V.; Semenov, A. I.; Vinokurov, N. A.; Kolchanov, N. A.; Popik, V. M.; Peltek, S. E. Studying the non-thermal effects of terahertz radiation on *E. coli* pKatG-GFP biosensor cells. *Bioelectromagnetics* **2013**, *34* (1), 15−21.
(28) Serdyukov, D. S.; Goryachkovskaya, T. N.; Mescheryakova, I. A.; Bannikova, S. V.; Kuznetsov, S. A.; Cherkasova, O. P.; Popik, V. M.; Peltek, S. E. Study on the effects of terahertz radiation on gene networks of *Escherichia coli* by means of fluorescent biosensors. *Biomed. Opt. Express* **2020**, *11* (9), 5258−5273.
(29) Meshcheryakova, I.; Goryachkovskaya, T.; Bannikova, S.; Rozanov, A.; Demidova, E.; Oshchepkov, D.; Demidov, E.; Bryanskaya, A.; Vinokurov, N.; Popik, V.et al. In *Construction of a Biosensor Sensitive to Terahertz Radiation Based on the Glutamine Synthetase Gene Promoter*, AIP Conference Proceedings; AIP, 2020.
(30) Serdyukov, D. S.; Goryachkovskaya, T. N.; Mescheryakova, I. A.; Kuznetsov, S. A.; Popik, V. M.; Peltek, S. E. Fluorescent bacterial biosensor *E. coli*/pTdcR-TurboYFP sensitive to terahertz radiation. *Biomed. Opt. Express* **2021**, *12* (2), 705−721.
(31) Peltek, S.; Meshcheryakova, I.; Kiseleva, E.; Oshchepkov, D.; Rozanov, A.; Serdyukov, D.; Demidov, E.; Vasiliev, G.; Vinokurov, N.; Bryanskaya, A.; et al. *E. coli* aggregation and impaired cell division after terahertz irradiation. *Sci. Rep.* **2021**, *11* (1), No. 20464.
(32) Bannikova, S.; Khlebodarova, T.; Vasilieva, A.; Mescheryakova, I.; Bryanskaya, A.; Shedko, E.; Popik, V.; Goryachkovskaya, T.; Peltek, S. Specific features of the proteomicresponse of thermophilic bacterium *Geobacillus icigianus* to terahertz irradiation. *Int. J. Mol. Sci.* **2022**, *23* (23), No. 15216.
(33) Barbora, A.; Rajput, S.; Komoshvili, K.; Levitan, J.; Yahalom, A.; Liberman-Aronov, S. Non-ionizing millimeter waves non-thermal radiation of *Saccharomyces cerevisiae*−Insights and Interactions. *Appl. Sci.* **2021**, *11* (14), No. 6635.
(34) Sitnikov, D. S.; Ilina, I. V.; Revkova, V. A.; Rodionov, S. A.; Gurova, S. A.; Shatalova, R. O.; Kovalev, A. V.; Ovchinnikov, A. V.; Chefonov, O. V.; Konoplyannikov, M. A.; et al. Effects of high intensity non-ionizing terahertz radiation on human skin fibroblasts. *Biomed. Opt. Express* **2021**, *12* (11), 7122−7138.
(35) Zhao, X.; Drlica, K. Reactive oxygen species and the bacterial response to lethal stress. *Curr. Opin. Microbiol.* **2014**, *21*, 1−6.
(36) Garcia-Moreno, A.; Lopez-Dominguez, R.; Villatoro-Garcia, J. A.; Ramirez-Mena, A.; Aparicio-Puerta, E.; Hackenberg, M.; Pascual-Montano, A.; Carmona-Saez, P. Functional enrichment analysis of regulatory elements. *Biomedicins* **2022**, *10* (3), No. 590.

https://doi.org/10.1021/acsomega.4c08710
ACS Omega 2024, 9, 49878−49886